

Article

Photo-Responsive Brominated Hydrogen-Bonded Liquid Crystals

Christian Anders ¹, Tejal Nirgude ¹, Ahmed F. Darweesh ² and Mohamed Alaasar ^{1,*}

¹ Department of Chemistry, Martin-Luther University Halle-Wittenberg, Kurt Mothes Str. 2, 06120 Halle (Saale), Germany; christian.anders@chemie.uni-halle.de (C.A.); tejal.nirgude@student.uni-halle.de (T.N.)

² Department of Chemistry, Faculty of Science, Cairo University, Giza 12613, Egypt; darweesh@sci.cu.edu.eg

* Correspondence: mohamed.alaasar@chemie.uni-halle.de

Abstract

This study reports on the preparation and comprehensive characterisation of new brominated hydrogen-bonded liquid crystalline (HBLC) materials. Two distinct series of supramolecular complexes were prepared by hydrogen-bond formation between 3-bromo-4-pentyloxybenzoic acid as the proton donor and non-fluorinated and fluorinated azopyridines with variable terminal chains as proton acceptors. The successful formation of a hydrogen bond was confirmed by FTIR spectroscopy. The impact of alkyl chain length and fluorination on the mesomorphic properties of the HBLCs was systematically investigated. The molecular self-assembly was thoroughly examined using polarised optical microscopy (POM) and differential scanning calorimetry (DSC), revealing the presence of smectic C (SmC), smectic A (SmA), and nematic (N) phases, with thermal stability being highly dependent on the molecular architecture. Notably, the introduction of fluorine atoms significantly influenced the phase transition temperatures and the overall mesophase range. Using bromine as a lateral substituent induces the formation of SmC phases in these HBLCs, a feature absent in their non-brominated analogues. Further structural insights were obtained through X-ray diffraction (XRD) investigations, confirming the nature of the observed LC phases. Additionally, the photo-responsive characteristics of these HBLCs were explored via UV-Vis spectroscopy, demonstrating their ability to undergo reversible photoisomerisation upon light irradiation. These findings underscore the critical role of precise molecular design in tailoring the properties of HBLCs for potential applications such as optical storage devices.

Keywords: azopyridine; bromine; hydrogen bonding; fluorine; liquid crystals



Academic Editors: Vladimir Chigrinov and Irina Cârlescu

Received: 1 October 2025

Revised: 10 October 2025

Accepted: 11 October 2025

Published: 14 October 2025

Citation: Anders, C.; Nirgude, T.; Darweesh, A.F.; Alaasar, M. Photo-Responsive Brominated Hydrogen-Bonded Liquid Crystals. *Crystals* **2025**, *15*, 886. <https://doi.org/10.3390/cryst15100886>

Copyright: © 2025 by the authors. Licensee MDPI, Basel, Switzerland. This article is an open access article distributed under the terms and conditions of the Creative Commons Attribution (CC BY) license (<https://creativecommons.org/licenses/by/4.0/>).

1. Introduction

Liquid crystals (LCs) represent a fascinating class of materials that combine the fluidity of liquids with the long-range order characteristic of crystalline solids. Their unique optical and electrical properties have made them indispensable in a wide array of technological applications, most notably in liquid crystal displays (LCDs) [1,2]. Beyond conventional display technologies, the continuous demand for advanced LC materials with enhanced functionalities has spurred extensive research into novel molecular designs and self-assembly strategies [3]. Among these, supramolecular approaches, particularly those utilising non-covalent interactions, such as hydrogen bonding [4–7] and halogen bonding [8–13], have emerged as successful tools for constructing complex and highly ordered LC architectures.

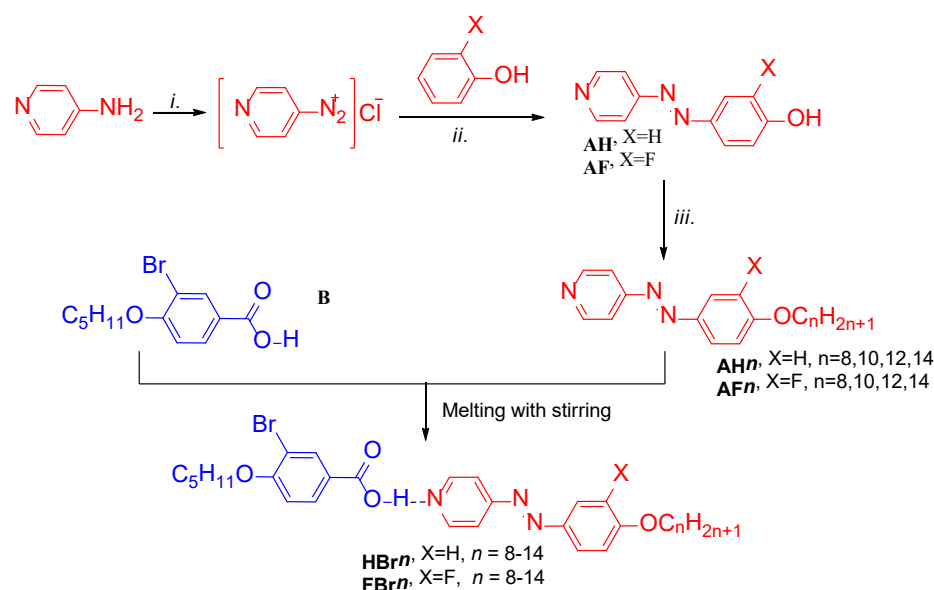
The reversible nature of hydrogen bonds also provides a pathway for dynamic and responsive LC systems, enabling the design of materials with tuneable properties. For instance, hydrogen bonding between pyridine derivatives and benzoic acid derivatives has been widely explored to generate diverse supramolecular liquid crystals with tailored mesophase behaviour [6]. H-bonding offers a versatile and robust mechanism for inducing and stabilising various mesophases, including conventional nematic [14–17], cybotactic nematic [18,19], twist bent nematic [20], smectic [18,19], columnar [21–23], and cubic phases [24,25].

When HBLCs are integrated with photo-responsive moieties, such as an azopyridine unit, they gain the ability to undergo light-driven conformational changes [10,25,26]. Azopyridine derivatives are particularly attractive in this context, as they combine the photo-responsive characteristics of azobenzenes with the capacity for self-assembly through intermolecular interactions. The *trans-cis* photoisomerisation of azopyridines can induce significant alterations in molecular shape and packing, leading to reversible phase transitions that are highly desirable for applications in photonics, optical data storage, and molecular switches [1,2].

Another crucial aspect in the design of advanced LC materials is the strategic incorporation of fluorine atoms into the molecular architecture. Fluorination is a well-established tool for modifying the mesophase behaviour of LCs due to the unique electronic and steric properties of fluorine [27]. The high electronegativity of fluorine can significantly influence molecular polarity and intermolecular interactions, while its relatively small size allows for subtle steric effects. The position and number of fluorine atoms can thus be precisely tuned to optimise mesophase stability, broaden nematic ranges, or even induce new polar phases [28–32].

Halogen bonding is another non-covalent interaction of growing importance in supramolecular LCs [8–12]. It involves a polarised halogen atom (e.g., bromine [8,9,33,34]) as an electron acceptor and a Lewis base (e.g., nitrogen in pyridine derivatives) as an electron donor. Bromine has also been used as a lateral substitution to design different types of thermotropic LCs, including photoresponsive ones [35–38]. Bromine is characterised by its larger crystal volume of Immirzi ($cv \sim 33 \text{ nm}^3$) [39] compared to that of the fluorine atom ($cv \sim 13 \text{ nm}^3$) [39], which leads to more steric interaction and in turn to different LC behaviour. However, to the best of our knowledge, the use of bromine as a lateral substituent in HBLCs has not yet been reported.

Building upon these foundational principles, herein we report the design, preparation, and comprehensive characterisation of the first examples of brominated HBLCs. Our primary objective is to systematically investigate the influence of varying alkyl chain lengths and the introduction of a fluorine atom as an additional lateral substituent on the mesomorphic and photo-responsive properties of these new HBLCs. Furthermore, we elucidated the effect of the lateral bromine atom by comparing the phase behaviour of one of the new HBLCs with that of a structurally related non-brominated HBLC [19] and a covalently bonded analogue [38]. To this end, we have prepared two distinct series of HBLCs—non-fluorinated (**HBrn**) and fluorinated (**FBrn**)—using 3-bromo-4-pentyloxybenzoic acid as the proton donor and two different types of azopyridine derivatives as proton acceptors (Scheme 1). The molecular self-assembly and mesomorphic properties were thoroughly examined using polarised optical microscopy (POM), differential scanning calorimetry (DSC), and X-ray diffraction (XRD), with hydrogen bond formation confirmed by FTIR spectroscopy. Finally, the *trans-cis* photoisomerisation of these HBLCs was also investigated. By combining these results, we elucidate the structure–property relationships in these new materials, offering valuable insights for the development of the next generation of functional HBLCs.



Scheme 1. Synthesis of the supramolecular complexes **HBr_n** and **FBr_n**. **Reagents and conditions:** *i.* NaNO₂/HCl/H₂O, 0 °C, 5h; *ii.* NaOH, NaHCO₃; *iii.* BrC_nH_{2n+1}, K₂CO₃, DMF, 80 °C, 18 h.

2. Materials and Methods

2.1. Synthesis

The hydrogen-bonded supramolecular complexes, designated as **HBr_n** and **FBr_n**, were synthesised according to Scheme 1. The synthesis of the proton donor, i.e., 3-bromo-4-pentyloxybenzoic acid, is reported in reference [40], while the synthesis of the azopyridine derivatives is noted in our previous reports [24,41]. The analytical data were in agreement with those previously reported, confirming the chemical structures [24,40,41]. As examples, the analytical data for 3-bromo-4-pentyloxybenzoic acid (**B**) and the azopyridine derivatives **AH14** and **AF14** are given below.

3-Bromo-4-pentyloxybenzoic acid (B): ¹H NMR (402 MHz, DMSO) δ 8.04 (d, *J* = 2.1 Hz, Ar-*H*, 1H), 7.90 (dd, *J* = 8.6, 2.1 Hz, Ar-*H*, 1H), 7.16 (d, *J* = 8.7 Hz, Ar-*H*, 1H), 4.10 (t, *J* = 6.4 Hz, O-CH₂-, 2H), 1.84–1.66 (m, OCH₂CH₂-, 2H), 1.50–1.24 (m, -CH₂-, 4H), 0.88 (t, *J* = 7.2 Hz, -CH₃, 3H). ¹³C NMR (101 MHz, DMSO) δ 166.31, 158.73, 134.22, 131.07, 124.54, 113.36, 111.15, 69.41, 40.31, 40.10, 39.89, 39.68, 39.48, 28.48, 28.01, 22.19, 14.29.

4-(4-Tetradecyloxyphenylazo)pyridine (AH14): ¹H NMR (600 MHz, CDCl₃) δ 8.77 (d, *J* = 5.9 Hz, Ar-*H*, 2H), 7.95 (d, *J* = 9.0 Hz, Ar-*H*, 2H), 7.67 (d, *J* = 6.0 Hz, Ar-*H*, 2H), 7.02 (d, *J* = 9.0 Hz, Ar-*H*, 2H), 4.06 (t, *J* = 6.6 Hz, -OCH₂-, 2H), 1.84–1.80 (m, -OCH₂CH₂-, 2H), 1.56–1.12 (m, -CH₂-, 22H), 0.88 (t, *J* = 7.0 Hz, CH₃, 3H). ¹³C NMR (151 MHz, CDCl₃) δ 162.89, 157.51, 151.01, 146.69, 125.62, 116.10, 114.93, 68.52, 31.92, 29.70, 29.61, 29.63, 29.49, 29.52, 29.32, 29.12, 25.88, 22.60, 14.12.

4-(3-Fluoro-4-tetradecyloxyphenylazo)pyridine (AF14): ¹H NMR (500 MHz, CDCl₃) δ 8.91–8.64 (m, Ar-*H*, 2H), 7.82 (ddd, *J* = 8.7, 2.4, 1.3 Hz, Ar-*H*, 1H), 7.72 (dd, *J* = 11.9, 2.3 Hz, Ar-*H*, 1H), 7.68–7.65 (m, Ar-*H*, 2H), 7.09 (t, *J* = 8.5 Hz, Ar-*H*, 1H), 4.14 (t, *J* = 6.6 Hz, -OCH₂-, 2H), 1.98–1.77 (m, OCH₂CH₂-, 2H), 1.53–1.15 (m, -CH₂-, 22H), 0.88 (t, *J* = 6.9 Hz, -CH₃, 3H). ¹³C NMR (126 MHz, CDCl₃) δ 157.07, 153.86, 151.88, 151.30, 151.24, 151.15, 146.23, 124.29, 116.15, 113.39, 107.89, 69.57, 31.90, 29.71–29.28 (m, 8C), 29.01, 25.86, 22.67, 14.09. ¹⁹F NMR (470 MHz, CDCl₃) δ −132.38 (dd, *J* = 11.9, 8.4 Hz).

The target final supramolecular complexes were obtained by precisely mixing equimolar amounts of the proton donor (**B**) and each of the azopyridine derivatives (**AH_n** and **AF_n**) over a glass slide, followed by heating with stirring until complete melting of the two components. The obtained liquid was allowed to cool down to room temperature. This

process was repeated twice to facilitate hydrogen bond formation and ensure homogeneity. The successful formation of the hydrogen-bonded complexes was subsequently verified through FTIR spectroscopy, polarised optical microscopy (POM), X-ray diffraction (XRD), and differential scanning calorimetry (DSC).

2.2. Characterisation

All synthesised compounds and their supramolecular complexes underwent complete characterisation using different techniques. All characterisation methods and their details can be found in the Supporting Information (SI) file.

3. Results and Discussion

3.1. FTIR Studies

The successful formation of the hydrogen bond between the benzoic acid derivative (proton donor, **B**) and the azopyridine derivatives (proton acceptors, **AH_n** and **AF_n** series) was proved via Fourier-transform infrared (FTIR) spectroscopy.

In the FTIR spectra, one of the most indicative changes associated with hydrogen bond formation is typically observed in the carbonyl (C=O) stretching region of the benzoic acid derivative [17–19]. As an example from the first group of the HBLCs, the FTIR spectra for the supramolecule **HBr12**, as well as for its individual components **B** and **AH12**, are shown in Figure 1a,b in two different regions. Upon complexation, a shift in the C=O stretching vibration of the carboxylic acid group to a higher wavenumber was expected. This was the case, as can be seen in Figure 1b, where the C=O stretching vibration wavenumber value changes from 1670 cm^{−1} in the pure acid **B** (blue curve) to 1702 cm^{−1} in the supramolecular complex **HBr12** (green curve). Another indication for the H-bond formation is the disappearance of the broad band observed for the pure acid **B** between 1800 and 3300 cm^{−1} (blue curve Figure 1a) and the appearance of two new broad bands in the lower wavenumber region of **HBr12** (2445 cm^{−1} and 1908 cm^{−1}, green curve Figure 1a), characteristic of the O–H stretching vibrations of the hydrogen-bonded complex [17,19].

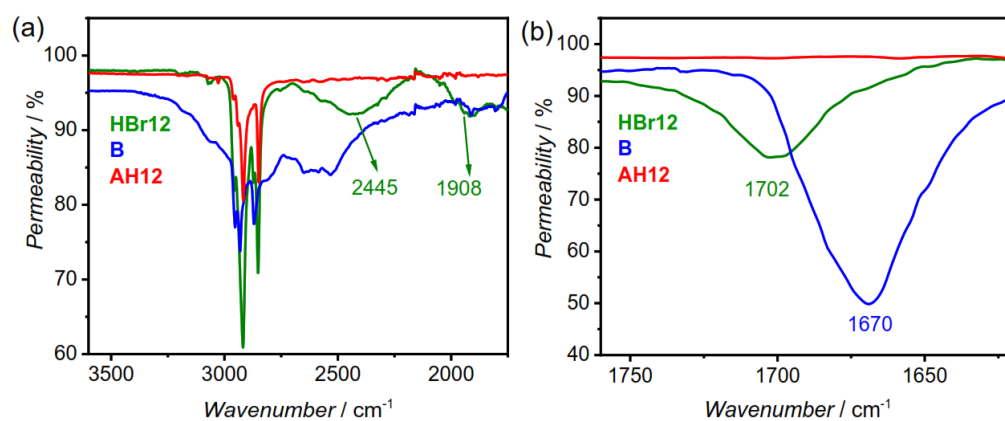


Figure 1. FTIR spectra of the supramolecule **HBr12** (green line) and its complementary components, pure acid **B** (blue line) and azopyridine derivative **AH12** (red line), in the crystalline state at room temperature: enlarged area between (a) 1750 cm^{−1} and 3600 cm^{−1} and (b) 1620 cm^{−1} and 1760 cm^{−1}.

These spectral changes confirm the interaction between the carboxylic acid proton and the pyridine nitrogen, leading to successful formation of the supramolecular H-bonded complex **HBr12**.

Similar results were also obtained for the second group of the fluorinated HBLCs with fluorinated azopyridines (**AF_n**) as the proton acceptors. As an example, the FTIR spectra of the H-bonded complex **FBr12**, as well as its individual components **AF12** and **B**, are shown

in Figure 2a,b. Again, a clear shift in the C=O vibration band before and after complexation can be observed ($1670\text{ cm}^{-1} \rightarrow 1702\text{ cm}^{-1}$, Figure 2b blue and green curves, respectively). Also, the appearance of the broad bands for **FBr12** at 2532 cm^{-1} and 1898 cm^{-1} (green curve Figure 2a) further confirms the formation of H-bonded materials.

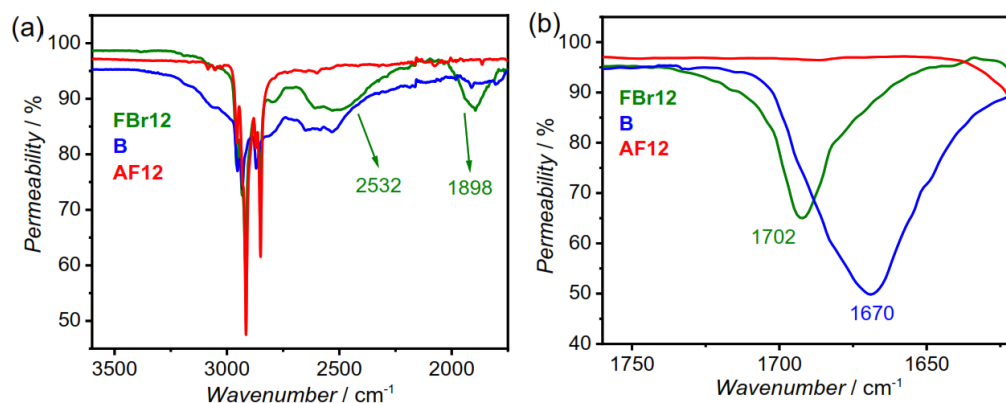


Figure 2. FTIR spectra of the supramolecule **FBr12** (green line) and its complementary components, acid **B** (blue line) and **AF12** (red line), in the crystalline state at room temperature: enlarged area between: (a) 1750 cm^{-1} and 3600 cm^{-1} and (b) 1620 cm^{-1} and 1760 cm^{-1} .

3.2. DSC and POM Investigations

The mesomorphic properties of the newly prepared hydrogen-bonded supramolecular complexes (**HBrn** and **FBrn** series) were extensively investigated using a combination of differential scanning calorimetry (DSC) and polarised optical microscopy (POM). The combined results from DSC and POM are summarised in Table 1 and represented graphically in Figure 3. The materials exhibit good thermal stability, as evidenced by the reproducibility of their transition temperatures over multiple DSC heating and cooling cycles.

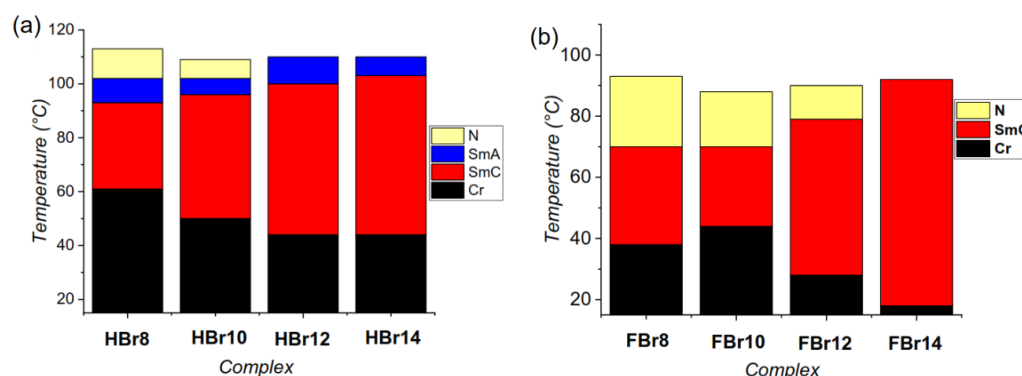
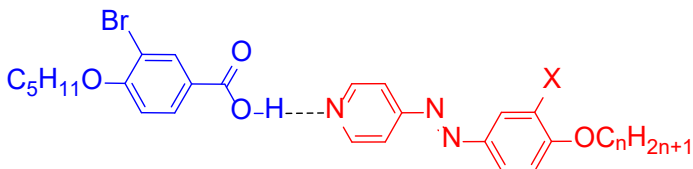


Figure 3. Bar diagram of the prepared complexes, (a) **HBrn** and (b) **FBrn**, as determined from POM and 2nd cooling DSC scans with a rate of 10 K min^{-1} . For abbreviations and numerical data when cooling, see Table 1.

It should be noted that both the proton donor (**B**) and each of the azopyridine derivatives (**AHn** and **AFn**) are non-mesomorphic and melt directly to the isotropic liquid state from the crystalline solid. Acid **B** has a melting point of $\sim 142\text{ }^{\circ}\text{C}$, while **AHn** and **AFn** have melting points ranging from $58\text{ }^{\circ}\text{C}$ to $74\text{ }^{\circ}\text{C}$ [19]. Upon their complexation, a rich variety of mesophases is induced, demonstrating the successful formation of a hydrogen bond between the two components and the presence of new hydrogen-bonded materials.

Table 1. Phase sequence with transition temperatures ($T/^{\circ}\text{C}$), mesophase types, and transition enthalpies [ΔH (kJ/mol)] of the H-bonded materials **HBrn** and **FBrn**^a.


Complex	n	X	Phase Sequence $T/^{\circ}\text{C}$ [$\Delta H/\text{kJ mol}^{-1}$]
HBr8	8	H	H: Cr 81 [28.7] SmC 96 [0.6] SmA 104 [1.1] N 116 [2.1] Iso C: Iso 113 [−2.3] N 102 [−0.8] SmA 93 [−1.2] SmC 61 [−25.8] Cr
HBr10	10	H	H: Cr 79 [13.3] SmC 100 [10.2] ^b SmA 107 [10.2] ^b 112 [10.2] Iso C: Iso 109 [−5.2] ^b N 102 [−5.2] ^b SmA 96 [−0.6] SmC 50 [−22.6] Cr
HBr12	12	H	H: Cr 63 [29.1] SmC 103 [1.6] SmA 112 [6.4] Iso C: Iso 110 [−7.0] SmA 100 [−0.6] SmC 44 [−19.9] Cr
HBr14	14	H	H: Cr 79 [46.4] SmC 106 [1.6] SmA 113 [7.8] Iso C: Iso 110 [−8.1] SmA 103 [−0.3] SmC 44 [−18.8] Cr
FBr8	8	F	H: Cr 80 [36.9] SmC 93 [0.6] N 106 [0.8] Iso C: Iso 93 [−1.2] N 70 [−0.9] SmC 38 [−23.4] Cr
FBr10	10	F	H: Cr 89 [46.2] N 103 [1.5] Iso C: Iso 88 [−1.4] N 70 [−0.5] SmC 44 [−22.6] Cr
FBr12	12	F	H: Cr 77 [57.7] SmC 90 [2.5] N 105 [2.8] Iso C: Iso 90 [−3.6] N 79 [−0.3] SmC 28 [41.0] Cr
FBr14	14	F	H: Cr 86 [72.1] SmC 105 [2.5] Iso C: Iso 92 [−4.7] SmC 18 [−37.7] Cr

^a Transition temperatures and enthalpy values were taken from the second DSC heating scans (10 K min^{-1}); ^b the transition enthalpy values cannot be separated; abbreviations: **H** = heating; **C** = cooling; Cr = crystalline state; SmC = smectic C phase; SmA = smectic A phase; N = nematic phase; and Iso = isotropic liquid phase.

3.2.1. Non-Fluorinated HBLCs (**HBrn**)

The non-fluorinated series of the hydrogen-bonded liquid crystalline materials (**HBrn**, where n represents the alkyl chain length at the azopyridine side) exhibits three different LC phases depending on n and temperature. As summarised in Table 1 and plotted in Figure 3, the shortest member of this series (**HBr8**) displays three LC phases, and all of them are of enantiotropic nature. This was confirmed from the DSC heating and cooling scans (Figure 4a), where the transition between the different mesophases was recorded before the transition to the isotropic (Iso) liquid state upon heating the crystalline state or upon cooling from the Iso liquid.

Optical textures investigations observed under POM (Figure 5) provided visual confirmation of the different mesophases. Therefore, when cooling from the Iso state under crossed polarisers, **HBr8** displayed a Schlieren texture that flashed when applying shearing stress, which is typically observed in the nematic (N) phase (Figure 5a). At the transition to the next LC phase, the highly birefringent texture of the N phase was replaced by dark texture with some bright points (Figure 5b), indicating the transition from N to SmA phase. With further cooling, the dark texture was replaced by another birefringent one, which is indicative of the SmA-SmC transition before the occurrence of crystallisation with further cooling. Therefore, the overall phase sequence of **HBr8** when cooling is Iso→N→SmA→SmC→Cr, which was also found when heating the sample again after reaching the crystalline state. This phase sequence was further confirmed by X-ray diffraction (XRD) investigations, as will be discussed later (Section 3.3).

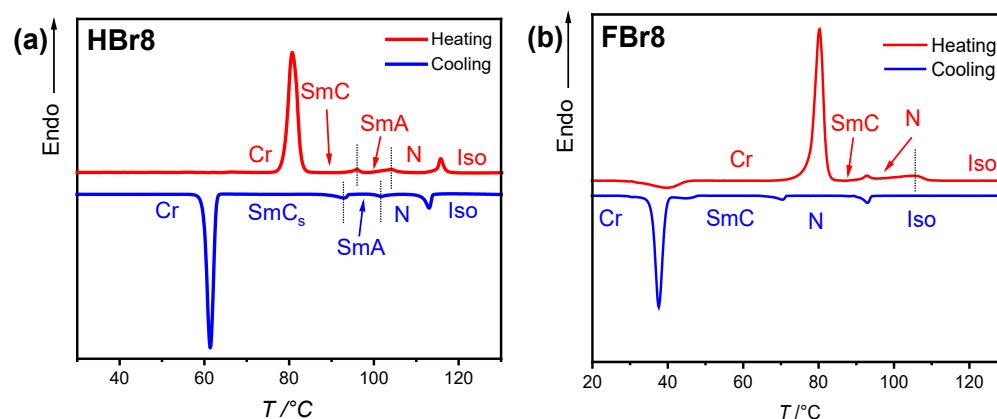


Figure 4. DSC thermograms recorded during the second heating and cooling scans for the supramolecular complexes: (a) **HBr8** and (b) **FBr8**, with heating and cooling rates of 10 K/min^{-1} .

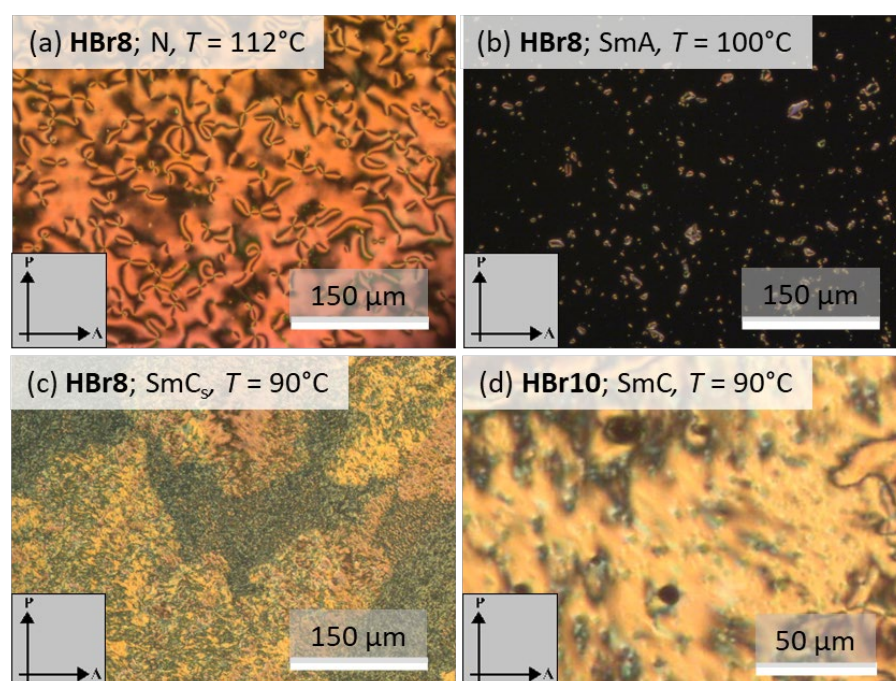


Figure 5. Optical textures observed when cooling from the Iso state at the indicated temperatures for (a) the Schlieren texture of the nematic phase of **HBr8**; (b) homeotropic area of the SmA phase of **HBr8**; (c) the birefringent texture of the SmC phase of **HBr8**; and (d) the SmC phase of **HBr10**. The arrows indicate the direction of the polarizer (P) and analyzer (A).

For the next homologue, **HBr10** with $n = 10$, a similar phase sequence as that of **HBr8** was observed. However, the melting and crystallisation temperatures of **HBr10** were reduced compared to those of **HBr8** because of chain elongation (Table 1). For the next two longer members, **HBr12** and **HBr14**, the melting point was decreased ($T = 63^\circ\text{C}$ for **HBr12**), then increased again ($T = 79^\circ\text{C}$ for **HBr14**). Also, the N phase was completely removed for both materials, while the SmA and SmC phases were retained. The crystallisation of both materials took place at $\sim T = 44^\circ\text{C}$, resulting in wide ranges of the LC phases compared to those of the shorter homologues.

Overall, the non-fluorinated HBLCs demonstrated a strong tendency to form smectic and nematic phases. The presence and stability of the N phase were influenced by the alkyl chain length, with **HBr8** and **HBr10** clearly exhibiting it, while it was absent for **HBr12** and **HBr14**. This suggests that the longer alkyl chains in **HBr12** and **HBr14** promote a more

ordered layered structure because of increased Van der Waals interactions between the hydrophobic segments.

3.2.2. Fluorinated HBLCs (**FBrn**)

The introduction of fluorine atoms into the azopyridine moiety in the case of the **FBrn** series significantly influenced the transition temperatures and mesomorphic behaviour of the HBLCs as compared to the **HBrn** series (Table 1 and Figure 3). Unlike their non-fluorinated counterparts, **FBrn** homologues exhibited SmC and N phases, with a general absence of the SmA phase observed for the **HBrn** series (Figure 3a,b). Additionally, the transition temperatures were significantly reduced, especially those for clearing and crystallisation in the case of **FBrn** materials (Figure 3a,b). This suggests that fluorination can disrupt the formation of the more ordered SmA layered structure.

The general observation of lower transition temperatures and the predominant absence of the SmA phase in the fluorinated series highlight the significant impact of fluorination on the mesomorphic properties. This effect is likely due to a combination of factors, including changes in dipole moment and intermolecular forces, all of which are influenced by the presence of the highly electronegative fluorine atom. This indicates how subtle structural modifications, such as fluorination, can be utilised to fine-tune the mesomorphic behaviour of HBLCs [15,19,41].

Optical textures obtained from POM (Figure 6) for the **FBrn** series confirm the presence of nematic and smectic C textures, consistent with the DSC data. The DSC thermograms (Figure 3b and Figure S2 in SI) for the **FBrn** series also clearly show the endothermic and exothermic peaks corresponding to the observed phase transitions. Across the **FBrn** series, the nematic phase had the largest range for the shortest homologue **FBr8**, with ~23 K when cooling. With chain elongation, this range decreased for the next members, **FBr10** and **FBr12**, to 18 K and 11 K, respectively. For the longest homologue **FBr14**, the nematic phase was completely removed, where the SmC was the only observed LC phase over the whole range, with a low crystallisation temperature of ~18 °C. This means that aromatic core fluorination in the case of these HBLCs could lead to room-temperature LC phases, which is of interest from an application point of view.

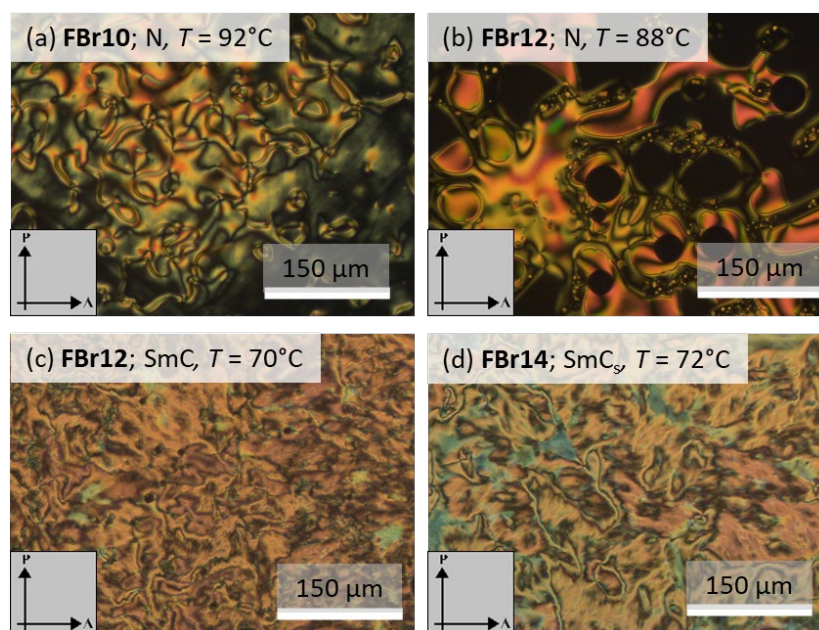


Figure 6. Optical textures observed when cooling from the Iso state at the indicated temperatures for (a) nematic droplets of **FBr10** at the transition from the Iso phase; (b) nematic phase of **FBr12**; (c) SmC phase of **FBr12**; and (d) SmC phase of **FBr14**.

3.3. XRD Investigations

X-ray diffraction (XRD) studies, including both Small-Angle X-ray Scattering (SAXS) and Wide-Angle X-ray Scattering (WAXS), were conducted on selected representative examples (**HBr8** and **FBr8**) to prove their LC phases and to corroborate the mesophase assignments derived from DSC and POM. The numerical SAXS data (Tables S1 and S2) and WAXS data (Tables S3 and S4) can be seen in the SI.

Figure 7 shows the WAXS patterns recorded for **HBr8** in the different LC phases. As can be seen, all WAXS results exhibit a broad halo scattering at $d \approx 0.43\text{--}0.45$ nm, corresponding to the lateral separation of the rigid aromatic cores, and confirming the presence of liquid crystal phases.

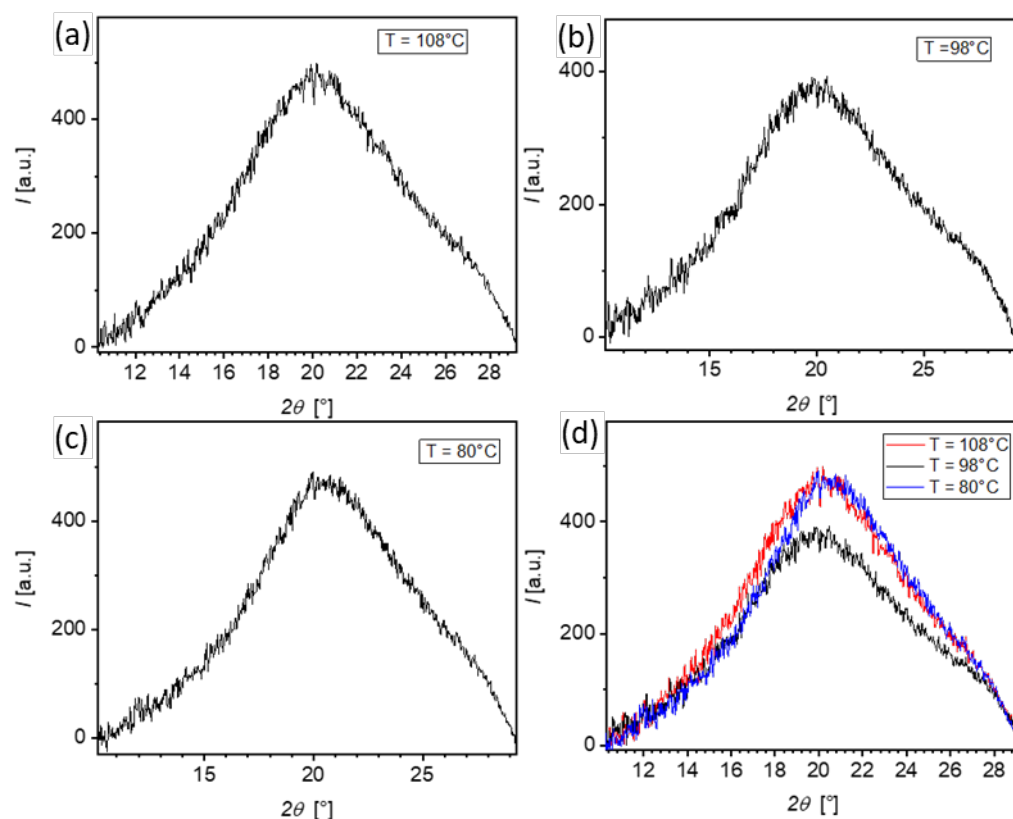


Figure 7. WAXS pattern recorded for **HBr8** when cooling at a rate of 10 K/min at the indicated temperatures: (a) N phase, (b) SmA phase, (c) SmC phase, and (d) comparison of the WAXS signals in different phases and temperatures.

The recorded SAXS patterns for the same complex are shown in Figure 8. When cooling from the Iso state and in the LC range of the nematic phase at $T = 111^\circ\text{C}$, a relatively broad single reflection could be observed (Figure 8a), which indicates the presence of a nematic phase. With further cooling, and at $T = 98^\circ\text{C}$, the single reflection became sharper, with a calculated layer spacing (d -spacing) of 3.59 nm, which corresponds to the molecular length ($L_{mol} = 3.58$ nm) calculated with Materials Studio (Figure 9). An additional second-order reflection can be observed at $2\theta = 4.96$. These data confirm the presence of orthogonal SmA phase, in line with the optical texture shown in Figure 5b. With further cooling, and at $T = 80^\circ\text{C}$, sharp first- and second-order reflections could still be recorded but with reduced layer spacing of $d = 2.96$ nm. This is significantly shorter than the molecular length, confirming the transition to a tilted lamellar phase i.e., SmC, which is also in agreement with the POM investigation (Figure 5c). Therefore, XRD investigations confirmed the phase sequence Iso \rightarrow N \rightarrow SmA \rightarrow SmC for **HBr8** when cooling.

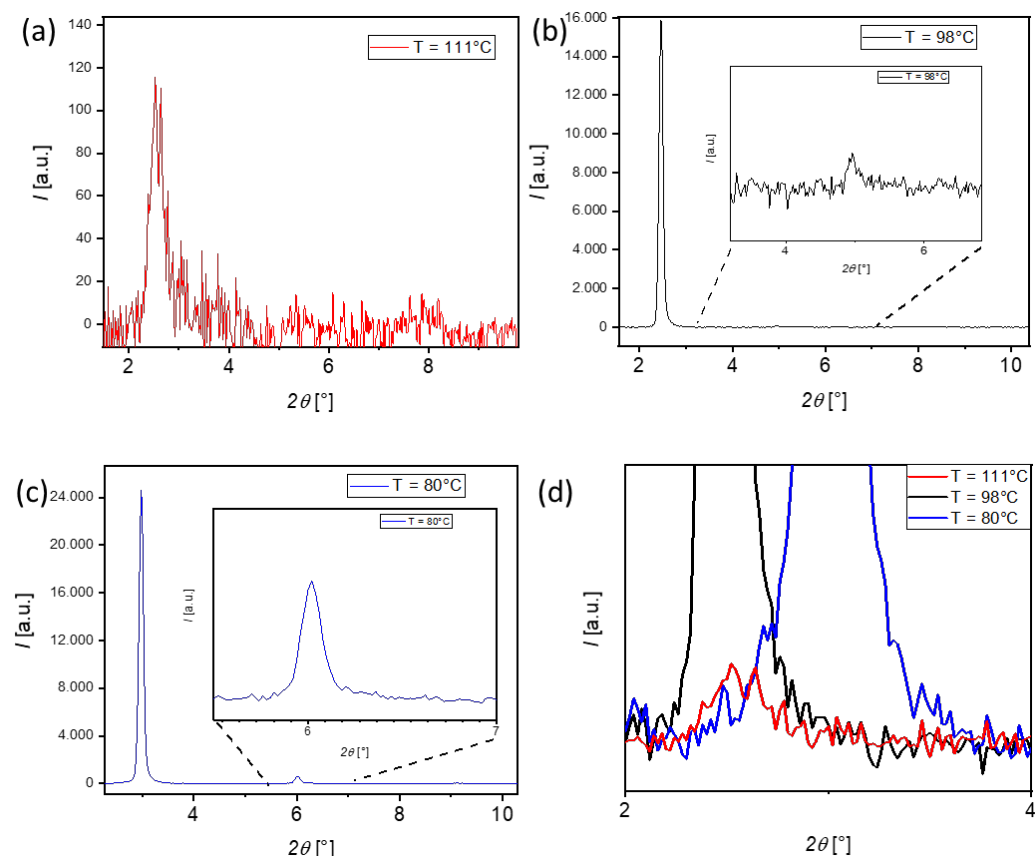


Figure 8. SAXS pattern for compound **HBr8** recorded when cooling at a rate of 10K/min at the indicated temperatures: (a) N phase; (b) SmA phase; (c) SmC phase; (d) relative peak shifts of the first reflexes for the recorded phases.

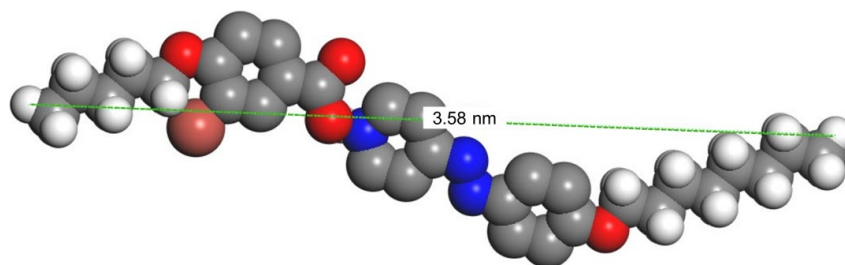


Figure 9. Space-filling model of the hydrogen-bonded complex **HBr8** showing the calculated molecular length (L_{mol}).

Investigations of the fluorinated analogue **FBr8** demonstrated the presence of the nematic phase at higher temperatures, followed by the SmC phase at lower temperatures (see Figure S3 and SI). These results are also in agreement with the observed optical textures (Figure 6).

From SAXS layer spacings and the calculated molecular lengths of the hydrogen-bonded complexes **HBr8** and **FBr8** ($L_{mol} = 3.58$ nm), tilt angles in the SmC phase of 33.6° for **HBr8** (80°C) (Table S1) and 31.0° for **FBr8** (60°C) (Table S2) were calculated according to $\theta = \cos^{-1}(d/L_{mol})$. The smaller tilt in the fluorinated complex correlates with a reduced lateral spacing observed in WAXS and is consistent with tighter in-plane packing induced by the polar F substituent.

3.4. Photoisomerisation Studies

The incorporation of an azopyridine unit within the molecular architecture of the **HBrn** and **FBrn** series of HBLCs grants these materials photo-responsive capabilities, namely the ability to undergo *trans-cis* photoisomerisation upon light irradiation. This light-induced conformational change is crucial for potential applications in optical data storage, molecular switches, and adaptive optical devices. The photoisomerisation behaviour of selected compounds with the same terminal chain length (**HBr8** and **FBr8**) was investigated using UV-Vis spectroscopy.

Upon UV light irradiation of **HBr8** in the LC phase, isothermal SmC-SmA, SmA-N or N-Iso transition could be achieved. These transitions took place in less than three seconds, i.e., fast, and were also reversible. Similar results were also obtained for the fluorinated material **FBr8**, where fast and reversible photoswitchable SmC-N and N-Iso transitions were achieved. These phase transitions could be explained as follows: under UV irradiation, the *trans* isomer of the azopyridine moiety undergoes photoisomerisation to its *cis* form. This *cis* isomer, being bent-shaped, typically disrupts the molecular packing and order within the LC phase, leading to a decrease in mesophase stability and therefore a transition to the next LC phase or even to the isotropic state.

The UV-Vis spectra of **HBr8** and **FBr8** in chloroform solution were also investigated, and the results are shown in Figure 10 (see also Figure S5 in the SI). A freshly prepared solution of both materials showed a strong absorption band at ~355 nm, corresponding to the π - π^* of the most stable *trans* isomer of the -N=N- unit. After light irradiation at different time intervals of five seconds, the band at 355 nm decreased, and another band at ~450 nm increased with time. The latter corresponds to n- π^* absorption of the less stable *cis* isomer. The *trans-cis* photoisomerisation was a reversible process, as indicated from the spectra obtained after irradiation of the solution, after keeping it in the dark overnight for 24 h, where a similar spectrum to that of the freshly prepared solution was obtained. This indicates the relaxation of the *cis* isomer to the *trans* one. The ability of these HBLCs to undergo reversible photoisomerisation suggests their potential for light-addressable applications.

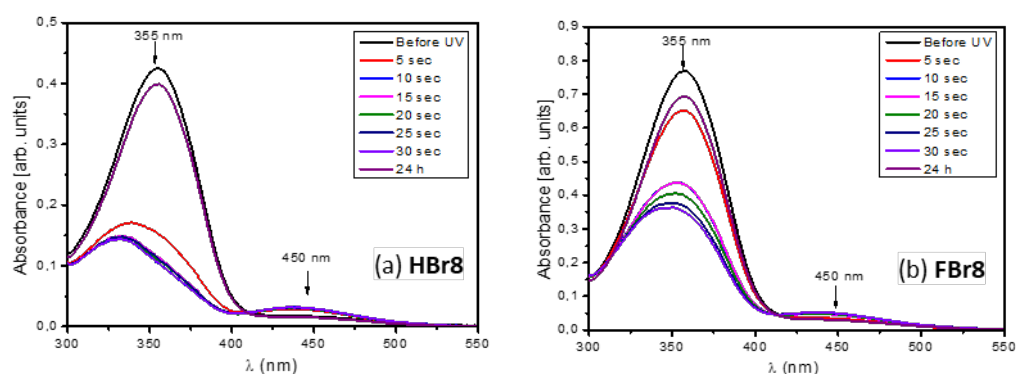


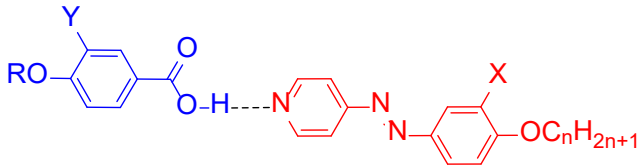
Figure 10. Spectral changes observed under UV light irradiation for (a) **HBr8** and (b) **FBr8** dissolved in chloroform, as recorded at room temperature.

3.5. Comparison with Related Materials

To understand the effect of aromatic core bromination on the phase behaviour in HBLCs, Table 2 shows a comparison between the newly reported materials (**HBr8** and **FBr8**) and their related HBLCs reported in the literature (**HH8** and **HF8**) [19]. Moreover, we have compared the phase behaviour of the covalently bonded material (**C8**, Figure 11) [38] with its related HBLC analogue (**FBr8**) to obtain more insight into the structure–property relationship in these materials. It should be noted that **HH8** and **HF8** each have a hexyloxy chain at the benzoic acid side, which means one more methylene (-CH₂-) group compared

to **HBr8** and **FBr8**. However, the comparison between these structures is still valid, as this additional $-\text{CH}_2-$ group cannot be the reason for the different phase behaviour compared to the effect of bromine substitution.

Table 2. Phase sequence and transition temperatures ($T/^{\circ}\text{C}$) of **HBr8** and **FBr8** in comparison to related materials [19]^a.



Complex	OR	X	Y	Phase Sequence $T/^{\circ}\text{C}$	Ref.
HH8	$-\text{OC}_6\text{H}_{13}$	H	H	H: Cr 106 SmA 124 N 134 Iso C: Iso 131 N 121 SmA 97 Cr	[19]
HBr8	$-\text{OC}_5\text{H}_{11}$	H	Br	H: Cr 81 SmC 96 SmA 104 N 116 Iso C: Iso 113 N 102 SmA 93 SmC 61 Cr	-
HF	$-\text{OC}_6\text{H}_{13}$	F	H	H: Cr 101 N 118 Iso C: Iso 115 N 84 Cr	[19]
FBr8	$-\text{OC}_5\text{H}_{11}$	F	Br	H: Cr 80 SmC 93 N 106 Iso C: Iso 93 N 70 SmC 38 Cr	-

^a Transition temperatures were taken from the second DSC heating scans (10 K min^{-1}); for abbreviations, see Table 1.

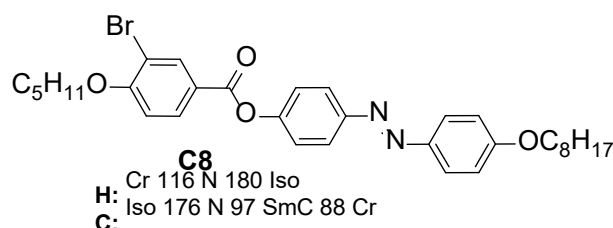


Figure 11. Chemical structure of the previously reported covalently bonded liquid crystal **C8** and its transition temperatures and phase types when heating (**H**) and cooling (**C**) [38].

Comparing the non-brominated HBLC **HH8** [19] with its brominated one (**HBr8**) indicates that bromination leads to a lower melting temperature and induces the formation of the SmC phase, which is absent for **HH8**. Also, the whole LC range after the cooling of **HBr8** ($\sim 52\text{ K}$) was wider than that of **HH8** (~ 34). This means that the introduction of a bromine atom as a lateral substitution did not suppress LC formation, despite its large size, but instead enhanced the mesophase range and induced new LC formation.

Similar observations were also observed when comparing the fluorinated HBLCs (**HF8** and **FBr8**). Again, the introduction of a bromine atom in the case of **FBr8** resulted in the induction of the SmC phase below the nematic one and a wider LC range compared to its non-brominated analogue, **HF8**.

On the other hand, comparing the covalently bonded LC material (**C8**, Figure 11) [38] with its HBLC analogue (**HBr8**) revealed that the clearing temperature of **C8** was higher than that of **HBr8**, resulting in a wider LC phase range. However, **C8** exhibited only a nematic phase with heating and additional SmC as a monotropic phase with the cooling cycle, while the HBLC analogue (**HBr8**) displayed polymorphism with a phase sequence of SmC-SmA-N after both heating and cooling. This suggests that the covalent linkage might restrict molecular movement or packing in a way that favours the nematic phase

and higher thermal stability, while the HBLC analogue, with its potentially more flexible structure, allows for the formation of more ordered smectic phases at lower temperatures.

4. Conclusions

In this study, we successfully designed, prepared, and characterised new brominated HBLCs, systematically exploring the impact of alkyl chain length and fluorination on their mesomorphic and photo-responsive properties. Two distinct series, non-fluorinated (**HBrn**) and fluorinated (**FBrn**) derivatives, were prepared through hydrogen-bond formation between a brominated benzoic acid derivative as a proton donor and various azopyridine derivatives as proton acceptors.

FTIR measurements confirmed the successful formation of the hydrogen bond between the complementary components. The LC behaviour, elucidated through DSC and POM, revealed a rich polymorphism, including SmC, SmA, and N phases. The influence of both alkyl chain length and fluorination on the observed phase sequences, transition temperatures, and mesophase stability was investigated. The non-fluorinated **HBrn** series exhibited high transition temperatures and a broad range of mesophases, including the SmA phase for certain chain lengths. In contrast, the fluorinated **FBrn** series showed a tendency towards lower transition temperatures and a predominant presence of SmC and N phases, suggesting that fluorination can modulate the intermolecular interactions and molecular packing, thereby influencing the overall mesomorphic behaviour.

Further structural insights were gained from XRD investigations, which confirmed the observed mesophases. The SAXS and WAXS data provided quantitative information on *d*-spacings and molecular packing, supporting the conclusions drawn from thermal and optical studies. Photoisomerisation studies demonstrated that these HBLCs are indeed photo-responsive, undergoing reversible *trans-cis* isomerisation of the azopyridine unit upon UV light irradiation. This inherent photoswitching capability highlights their potential for optical applications. Finally, a comparison between the new materials and previously reported ones provided useful insights about the effect of core bromination in HBLCs. It was demonstrated that lateral bromine substitution is directly responsible for inducing SmC phase, which was not observed in closely related non-brominated materials.

Overall, this research underscores the importance of careful molecular design, using different factors such as aromatic core bromination and fluorination, as well as terminal alkyl chain length, in tailoring the properties of HBLCs. These new HBLCs could be used for applications in optical data storage devices due to their photo-responsive behaviour.

Supplementary Materials: The following supporting information can be downloaded at <https://www.mdpi.com/article/10.3390/cryst15100886/s1>: Figure S1: DSC as recorded from second heating and cooling cycles of (a) **HBr10**, (b) **HBr12**, and (c) **HBr14** at a scanning rate of 10 °C/min; Figure S2: DSC as recorded from second heating and cooling cycles of (a) **FBr10**, (b) **FBr12**, and (c) **FBr14** at a scanning rate of 10 °C/min.; Figure S3: SAXS pattern of **FBr8** recorded after cooling at a rate of 10K/min at the indicated temperatures: (a) N phase; (b) SmC phase; (c) relative peak shifts of the first reflexes for the recorded phases; Figure S4: WAXS pattern of **FBr8** recorded after cooling at a rate of 10K/min at the indicated temperatures: (a) N phase; (b) SmC phase; (c) comparison of the WAXS signals in the different indicated phases and temperatures; Figure S5: Spectral changes observed under UV light irradiation for **HBr10**; Table S1: Numerical SAXS data of **HBr8**; Table S2: Numerical SAXS data of **FBr8**; Table S3: Numerical WAXS data of **HBr8**; Table S4: Numerical WAXS data of **FBr8**.

Author Contributions: Conceptualisation, writing—original draft preparation, writing—review and editing, supervision, funding acquisition, M.A.; methodology, validation, writing—original draft preparation, data curation, C.A. and M.A.; methodology, preparation, data curation, A.F.D. and T.N. All authors have read and agreed to the published version of the manuscript.

Funding: This research was funded by the German Research Foundation (DFG) (AL2378/1-2, 424355983, RTG 2670, 436494874) and the Alexander von Humboldt Foundation.

Data Availability Statement: The original contributions presented in the study are included in the article and Supplementary Materials; further inquiries can be directed to the corresponding author.

Conflicts of Interest: The authors declare no conflicts of interest. The funders had no role in the design of the study; in the collection, analyses, or interpretation of data; in the writing of the manuscript; or in the decision to publish the results.

References

- Kato, T.; Uchida, J.; Ichikawa, T.; Sakamoto, T. Functional Liquid Crystals Towards the Next Generation of Materials. *Angew. Chem.* **2018**, *57*, 4355–4371. [\[CrossRef\]](#)
- Bisoyi, H.K.; Li, Q. Liquid Crystals: Versatile Self-Organized Smart Soft Materials. *Chem. Rev.* **2022**, *122*, 4887. [\[CrossRef\]](#)
- Kato, T.; Kamikawa, Y. *Handbook of Liquid Crystals*; Goodby, J.W., Collings, P.J., Kato, T., Tschierske, C., Gleeson, H., Raynes, P., Eds.; Wiley-VCH: Weinheim, Germany, 2014; Volume 5, pp. 513–540.
- Kato, T.; Fréchet, J.M.J. A new approach to mesophase stabilization through hydrogen bonding molecular interactions in binary mixtures. *J. Am. Chem. Soc.* **1989**, *111*, 8533–8534. [\[CrossRef\]](#)
- Paleos, C.M.; Tsiourvas, D. Supramolecular hydrogen-bonded liquid crystals. *Liq. Cryst.* **2001**, *28*, 1127–1161. [\[CrossRef\]](#)
- Devadiga, D.; Ahipa, T.N. Recent synthetic advances in pyridine-based thermotropic mesogens. *RSC Adv.* **2019**, *9*, 23161–23228. [\[CrossRef\]](#)
- Yadykova, A.Y.; Konstantinov, I.I.; Vlasova, A.V.; Varfolomeeva, L.A.; Ilyin, S.O. Alkylbenzoic and Alkyloxybenzoic Acid Blending for Expanding the Liquid Crystalline State and Improving Its Rheology. *Int. J. Mol. Sci.* **2023**, *24*, 15706. [\[CrossRef\]](#)
- Du, M.; Li, L.; Zhang, J.; Li, K.; Cao, M.; Mo, L.; Hu, G.; Chen, Y.; Yu, H.; Yang, H. Photoresponsive Iodine-Bonded Liquid Crystals Based on Azopyridine Derivatives with a Low Phase-Transition Temperature. *Liq. Cryst.* **2019**, *46*, 37–44. [\[CrossRef\]](#)
- Chen, Y.; Yu, H.; Zhang, L.; Yang, H.; Lu, Y. Photoresponsive Liquid Crystals Based on Halogen Bonding of Azopyridines. *Chem. Commun.* **2014**, *50*, 9647–9649. [\[CrossRef\]](#) [\[PubMed\]](#)
- Alaasar, M.; Poppe, S.; Tschierske, C. Photoresponsive halogen bonded polycatenar liquid crystals. *J. Mol. Liq.* **2019**, *277*, 233–240. [\[CrossRef\]](#)
- Kumar, V.; Mulder, D.J.; Cavallo, G.; Pilati, T.; Terraneo, G.; Resnati, G.; Schenning, A.P.H.J.; Metrangolo, P. Structural Characterization of New Fluorinated Mesogens Obtained through Halogen-Bond Driven Self-Assembly. *J. Fluorine Chem.* **2017**, *198*, 54–60. [\[CrossRef\]](#)
- Bruce, D.W.; Metrangolo, P.; Meyer, F.; Prasang, C.; Resnati, G.; Terraneo, G.; Whitwood, A.C. Mesogenic, Trimeric, Halogen-Bonded Complexes from Alkoxystilbazoles and 1,4-Diodotetrafluorobenzene. *New J. Chem.* **2008**, *32*, 477–482. [\[CrossRef\]](#)
- Fernandez-Palacio, F.; Poutanen, M.; Saccone, M.; Siiskonen, A.; Terraneo, G.; Resnati, G.; Ikkala, O.; Metrangolo, P.; Priimagi, A. Efficient Light-Induced Phase Transitions in Halogen-Bonded Liquid Crystals. *Chem. Mater.* **2016**, *28*, 8314–8321. [\[CrossRef\]](#) [\[PubMed\]](#)
- Alaasar, M.; Tschierske, C.; Prehm, M. Hydrogen-bonded supramolecular complexes formed between isophthalic acid and pyridine-based Derivatives. *Liq. Cryst.* **2011**, *38*, 925–934. [\[CrossRef\]](#)
- Kappelt, A.; Giese, M. Photo-switchable Fluorescence in Hydrogen-Bonded Liquid Crystals. *Chem. Eur. J.* **2020**, *26*, 13347–13351. [\[CrossRef\]](#) [\[PubMed\]](#)
- Alaasar, M.; Tschierske, C. Nematic phases driven by hydrogen-bonding in liquid crystalline nonsymmetric dimers. *Liq. Cryst.* **2019**, *46*, 124–130. [\[CrossRef\]](#)
- Anders, C.; Abu Bakar, M.; Nirgude, T.; Alaasar, M. Nematic Phases in Photo-Responsive Hydrogen-Bonded Liquid Crystalline Dimers. *Crystals* **2025**, *15*, 576. [\[CrossRef\]](#)
- Arakawa, Y.; Sasaki, Y.; Igawa, K.; Tsuji, H. Hydrogen bonding liquid crystalline benzoic acids with alkylthio groups: Phase transition behavior and insights into the cybotactic nematic phase. *New J. Chem.* **2017**, *41*, 6514–6522. [\[CrossRef\]](#)
- Darweesh, A.F.; Anders, C.; Ranjitha, B.S.; Shanker, G.; Alaasar, M. On the impact of aromatic core fluorination in hydrogen-bonded liquid crystals. *RSC Adv.* **2025**, *15*, 6803–6816. [\[CrossRef\]](#)
- Jansze, S.M.; Martínez-Felipe, A.; Storey, J.; Marcelis, A.; Imrie, C.T. A Twist-Bend Nematic Phase Driven by Hydrogen Bonding. *Angew. Chem.* **2015**, *54*, 643–646. [\[CrossRef\]](#)
- Goldmann, D.; Janietz, D.; Schmidt, C.; Wendorff, J.H. Columnar liquid crystalline phases through hydrogen bonding and nanoscale segregation. *J. Mater. Chem.* **2004**, *14*, 1521–1525. [\[CrossRef\]](#)
- Chen, M.; Zhang, T.-R.; Yu, W.-H.; Li, Q.-G.; Xiang, S.-K.; Cao, P.; Zhao, K.-Q.; Feng, C.; Wang, B.-Q. Hydrogen-bonding stabilized columnar mesophases in hexasubstituted triphenylene 2,3-Dicarboxamides. *J. Mol. Liq.* **2022**, *366*, 120122. [\[CrossRef\]](#)

23. Martínez-Bueno, A.; Martín, S.; Ortega, J.; Folcia, C.L.; Termine, R.; Golemme, A.; Giménez, R.; Sierra, T. Effect of Hydrogen Bonding and Chirality in Star-Shaped Molecules with Peripheral Triphenylamines: Liquid Crystal Semiconductors and Gels. *Chem. Mater.* **2024**, *36*, 4343–4356. [\[CrossRef\]](#)
24. Alaasar, M.; Poppe, S.; Dong, Q.; Liu, F.; Tschierske, C. Mirror symmetry breaking in cubic phases and isotropic liquids driven by hydrogen bonding. *Chem. Commun.* **2016**, *52*, 13869–13872. [\[CrossRef\]](#)
25. Alaasar, M.; Schmidt, J.C.; Cai, X.; Liu, F.; Tschierske, C. Controlling liquid and liquid crystalline network formation by core-fluorination of hydrogen bonded supramolecular polycatenars. *J. Mol. Liq.* **2021**, *332*, 115870. [\[CrossRef\]](#)
26. Pfletscher, M.; Wölper, C.; Gutmann, J.S.; Mezger, M.; Giese, M. A modular approach towards functional supramolecular aggregates—Subtle structural differences inducing liquid crystallinity. *Chem. Commun.* **2016**, *52*, 8549–8552. [\[CrossRef\]](#)
27. Hird, M. Fluorinated liquid crystals: Properties and applications. *Chem. Soc. Rev.* **1992**, *21*, 147–154. [\[CrossRef\]](#)
28. Alaasar, M.; Prehm, M.; Tschierske, C. Mirror symmetry breaking in fluorinated bent-core mesogens. *RSC Adv.* **2016**, *6*, 82890–82899. [\[CrossRef\]](#)
29. Saccone, M.; Kuntze, K.; Ahmed, Z.; Siiskonen, A.; Giese, M.; Priimagi, A. *ortho*-Fluorination of azophenols increases the mesophase stability of photoresponsive hydrogen-bonded liquid crystals. *J. Mater. Chem. C.* **2018**, *6*, 9958–9963. [\[CrossRef\]](#)
30. Karcz, J.; Herman, J.; Rychłowicz, N.; Kula, P.; Górecka, E.; Szydłowska, J.; Majewski, P.W.; Pociecha, D. Spontaneous chiral symmetry breaking in polar fluid-heliconical ferroelectric nematic phase. *Science* **2024**, *384*, 1096–1099. [\[CrossRef\]](#)
31. Gibb, C.J.; Hobbs, J.; Nikolova, D.I.; Raistrick, T.; Berrow, S.R.; Mertelj, A.; Osterman, N.; Sebastián, N.; Gleeson, H.F.; Mandle, R.J. Spontaneous symmetry breaking in polar fluids. *Nat. Commun.* **2024**, *15*, 5845. [\[CrossRef\]](#)
32. Inui, S.; Kitaoka, H.; Eguchi, Y.; Yasui, M.; Konno, T.; Yamada, S. Design of Near-UV Photoluminescent Liquid-Crystalline Dimers: Roles of Fluorinated Aromatic Ring Position and Flexible Linker. *Crystals* **2025**, *15*, 840. [\[CrossRef\]](#)
33. Devadiga, D.; Ahipa, T.N. An up-to-date review on halogen-bonded liquid crystals. *J. Mol. Liq.* **2021**, *333*, 115961. [\[CrossRef\]](#)
34. Prasang, C.; Bruce, D.W. Halogen-Bonded Liquid Crystals. *Helv. Chim. Acta* **2023**, *106*, e202300008. [\[CrossRef\]](#)
35. Podoliak, N.; Novotná, V.; Kašpar, M.; Hamplová, V.; Glogarová, M.; Pociecha, D. Anomalous phase sequence in new chiral liquid crystalline materials. *Liq. Cryst.* **2014**, *41*, 176–183. [\[CrossRef\]](#)
36. Podoliak, N.; Hamplová, V.; Kašpar, M.; Novotná, V.; Glogarová, M.; Pociecha, D.; Gorecka, E. High tilted smectogens with bromine-substituted molecular core. *Liq. Cryst.* **2013**, *40*, 321–328. [\[CrossRef\]](#)
37. Takanishi, Y.; Nishiyama, I.; Yamamoto, J.; Ohtsuka, Y.; Iida, A. Remarkable effect of a lateral substituent on the molecular ordering of chiral liquid crystal phases: A novel bromo-containing dichiral compound showing SmC* variants. *J. Mater. Chem.* **2011**, *21*, 4465–4469. [\[CrossRef\]](#)
38. Alaasar, M.; Nirgude, T.; Anders, C. The influence of bromine substitution and linking groups on the phase behaviour of light-responsive rod-like molecules. *J. Mol. Liq.* **2024**, *414*, 126174. [\[CrossRef\]](#)
39. Immirzi, A.; Perini, B. Prediction of density in organic crystals. *Acta Cryst.* **1977**, *A33*, 216. [\[CrossRef\]](#)
40. Dingding, G.; Keting, B.; Mingming, Z.; Yingxia, L. Design, Synthesis and Biological Evaluation of Small-Molecule Inhibitors of Signal Transducer and Activator of Transcription#br# 3 (STAT3) Signaling Pathway. *Chin. J. Org. Chem.* **2016**, *36*, 1854–1862.
41. Alaasar, M.; Schmidt, J.-C.; Darweesh, A.F.; Tschierske, C. Azobenzene-based supramolecular liquid crystals: The role of core fluorination. *J. Mol. Liq.* **2020**, *310*, 113252. [\[CrossRef\]](#)

Disclaimer/Publisher's Note: The statements, opinions and data contained in all publications are solely those of the individual author(s) and contributor(s) and not of MDPI and/or the editor(s). MDPI and/or the editor(s) disclaim responsibility for any injury to people or property resulting from any ideas, methods, instructions or products referred to in the content.